Teknisia
Vol. 28, No. 2, November 2023, pp. 079-089
E-ISSN: 2746-0185

Investigation of effective section reduction in low carbon steel during SMAW welding

Malik Mushthofa[1,3,*], Fakhri Pratama Nurfauzi[2], Astriana Hardawati[1]
[1] Department of Civil Engineering, Faculty of Civil Engineering and Planning, Universitas Islam Indonesia, Indonesia
[2] PT Jaya Construction Management (Jaya CM), Indonesia
[3] Disaster Risk Reduction Center (DiRReC), Universitas Islam Indonesia, Indonesia

Article Info

Article history:

Received: 3 November 2023
Revised: 6 December 2023
Accepted:
16 December 2023
Available online:
30 December 2023

Keywords:

Welding
Heat affected zone
Distortion
Residual stress
Peak temperature

Corresponding Author:

Malik Mushthofa
185111302@uii.ac.id

Abstract

Welding, with its advantages of expedient execution and reduced weight, is a favored method for structural connections. However, it poses a significant risk, softening the steel and diminishing load-bearing capacity, underscoring the importance of accurate estimation. The need for precision is paramount, as critical infrastructure must remain operational not only during disasters but also during repair and maintenance activities. To address this challenge, this research introduces an approach to estimate the extent of capacity reduction resulting from welding, providing engineers with valuable insights for maintaining these critical systems structural integrity and functionality. The study examined low-carbon steel with various thicknesses, focusing on Heat Affected Zone (HAZ) width calculations and Abaqus simulations. Welding was performed at a speed of 1.67 cm/s with a 5 mm element increment. This research aimed to investigate the impact of welding parameters on low-carbon steel, particularly concerning HAZ measurements. A 4 mm-thick plate generated a 38.73 mm affected zone, while simulations with 5 mm to 12 mm thicknesses produced progressively narrower affected zones. Results demonstrated that steel plate thickness significantly influences the affected zone width, with thicker plates yielding narrower affected zones.

Background

Steel structures have become a prominent choice (Roy et al., 2022) for both primary and ancillary elements in civil engineering constructions (Andreotti et al., 2023). Various steel elements within civil engineering structures are unified through connections, including welding, bolted connections, rivets, and others. Structures employing welded connections are often preferred due to their expeditious execution and the overall reduction in weight compared to bolted connection systems (Nursani et al., 2020). Conversely, structures employing bolted connections are favored (Khan et al., 2023) for their ease of disassembly and reassembly (Liew et al., 2019), and reduced installation risks. However, bolted connections have the drawback of necessitating the creation of holes in the components or sections being joined (Wibowo et al., 2012).

As previously mentioned, supporting structures in civil engineering can be exemplified by structures like water towers in hospitals. At certain times, supporting structures such as water towers may require capacity expansion due to various factors related to the hospital's capacity needs. Capacity expansion, in other words, involves increasing the water storage capacity. In some cases, this must be achieved within the constraints of existing structures due to land limitations. Expanding

the water storage capacity leads to an increase in the load-bearing area of the structure, necessitating the addition of new elements that must be integrated with the existing structural elements.

Referring to SNI 1726: 2019, public facilities such as hospitals and several other essential amenities fall into the category of critical infrastructure, and they remain resilient in the face of disasters. Some public facilities can not cease operations during disasters (Nia & Kulatunga, 2017) or while undergoing maintenance. Based on this premise, structural elements should be added, particularly in buildings classified as critical structures, when the structure is load-bearing or during a service condition (Ahola et al., 2023).

As previously elucidated, one of the connection systems in steel structures is the welding connection system. Welding is a material joining process that produces coalescence at the welding interface through heating to a suitable temperature with or without the application of pressure or filler metal (Jeffus, 2017) as cited in (Arifin & Hendrianto, 2018), is a crucial technique. The bonding process through welding is executed by heating at a specific point, where the heating and cooling rates are relatively rapid (Arifin & Hendrianto, 2018). A rise in temperature within the steel elements can pose a substantial risk when the structure is load-bearing, as the introduction of heat can potentially soften the steel, thereby reducing its load-bearing capacity (Szymczak et al., 2020).

Many researchers have investigated the fire behavior of structures, and from the perspective of individual elements, much research is available on the mechanical properties of welded joints. Steel structures under fire face a relentless assault on their integrity. Rezaeian et al. (2020) observed a 550°c furnace reducing the tensile strength of S355 steel by a staggering 50%. This weakening is not limited to strength; Wang et al. (2019) reported beam-to-column connections experiencing a 60% stiffness drop at 600°C. As Wu et al. (2021) documented, the heat also induces unruly deformations, with steel beams warping out-of-plane under the fire's influence. Li et al. (2020) delved deeper, examining trusses and highlighting the potential instability lurking in bowing effects. Columns, too, are not spared. Yu et al. (2018) analyzed their buckling behavior at elevated temperatures, identifying critical slenderness ratios that spell disaster. Fahmy et al. (2019) sounded the alarm for welded connections, emphasizing their vulnerability to strength loss and premature failure when flames lick at their seams. However, the danger does not stop at the material level. Liu et al. (2019) showed how residual stresses within welds act like tiny saboteurs, amplifying thermal stresses and accelerating the formation of cracks. There is a gap in research regarding the effective area reduction of welded joints in steel structures due to temperature enhancement during weld.

This research offers an estimate or approach that engineers can utilize to assess the extent of structural capacity reduction arising from incorporating structural elements through welding. In the case of water towers, as previously exemplified, this estimate can serve as the basis for determining the maximum allowable water storage capacity during the welding process. Generally, the approach allows for calculating the remaining section's functional effectiveness as a portion of the gross section. The referenced approach is expected to underpin decision-making by engineers, facilitating task completion while ensuring the structure's continued effective operation.

Heat-affected zone (HAZ)

The heat-affected zone (HAZ) is the region where temperatures reach a level insufficient for melting but still reach a point where they induce significant alterations in the material's microstructure and properties (Kou, 2003). In a schematic representation, the division of zones formed during welding is illustrated in Figure 1.

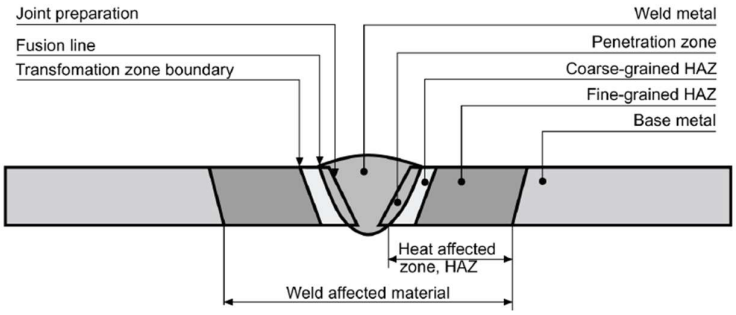

Figure 1. Heat affected zone division during welding (Weman, 2003)

It is essential to determine the thermal conditions within and around the weld metal in the context of welding. Of particular significance in this context are three specific factors:

1. the determination of the maximum temperature distribution in the heat-affected zone (HAZ) of the weld,
2. the assessment of cooling rates within both the weld metal and the heat-affected zone, and
3. the evaluation of the rate at which the weld metal undergoes solidification.

To accurately predict or comprehend the metallurgical transformations occurring at a specific location in solid metal near a weld, it is imperative to have access to information regarding the maximum temperature reached at that particular point. The temperature distribution in the base metal adjacent to a single-pass, full-penetration butt weld in sheet or plate materials can be described as follows (Weiss et al., 1976):

$$\frac{1}{T_p - T_o} = \frac{4.13\ \rho\ C_t\ Y}{H_{net}} + \frac{1}{T_m - T_o} \qquad (1)$$

T_p = the peak or maximum temperature, °C, at a distance, Y (mm), from the weld fusion boundary. (The peak temperature equation does not apply at points within the weld metal, but only in the adjacent heat-affected zone.); 1800
T_o = initial uniform temperature of the sheet or plate, °C; 25
T_m = melting temperature, °C (specifically, liquidus temperature of the metal being welded); 1540
H_{net} = net energy input; 419 J/mm
ρ = density of material, g/mm3; 0.0079
C = specific heat of solid metal, J/g.°C; 0.466
ρC = volumetric specific heat, J/mm3.°C; 0.0036814
t = thickness of solid or plate, mm; 4

$$H_{net} = \frac{f_1 EI}{V} \qquad (2)$$

E = volts; 35 V
I = amperage; 250 A
V = travel velocity of heat source; 1.67 mm/detik
f_1 = heat transfer efficiency; 0.8 for SMAW

Analysis method

In this study, low-carbon steel with a thickness of 4 mm was employed. The method involved the calculation of the Heat Affected Zone (HAZ) width as the initial step. Subsequently, simulations were carried out using Abaqus. The simulations were conducted with a welding speed of 5 mm per 30 seconds or 1.67 cm/s, while considering an element increment of 5 mm, concerning the parameters listed in Table 1. Thus, this research aims to investigate the effects of the welding process with these parameters on low-carbon steel, with a specific focus on measuring the HAZ.

Tabel 1. Reference parameter of heat flux simulation

Input	Nilai	SI
Mass Density	7850	kg/m^3
Young Modulus	2.00E+11	N/m^2
Poison ratio	0.30	
Expansion coef. alpha	1.14E-05	/ºC
Yield Stress	2.45E+08	N/m^2
Plastic Strain	0.20	
Conductivity	45	W/mºC
Specific heat capacity	466	J/kgºC
Boltzmann constant	1.38E-23	J/K
Peak Temperature	1500	ºC
Heat Flux	4.58E+10	W/m^2

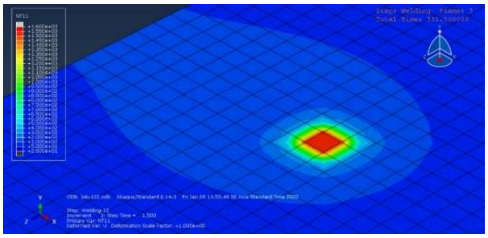

(a)

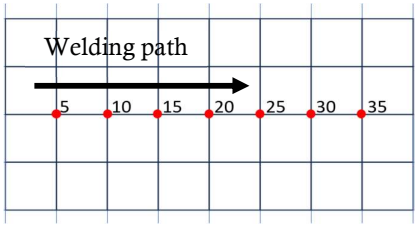

(b)

Figure 2. (a) Welding simulation in Abaqus; (b) Welding path simulation

Result and discussion

Temperature during welding

The graph (Figure 3) illustrates temperature variations at each nodal point during welding. Monitoring was conducted at nodal points 5, 10, 15, 20, 25, 30, and 35. The graph reveals that when welding reaches nodal point 5 (at 30 seconds), the temperature at nodal point 10 also experiences an increase. Subsequently, as the welding reaches nodal point 10 (at 60 seconds), the temperature at nodal point 5 remains high but begins to decrease. The temperature at nodal point 5 only stabilizes (no longer influenced) when the welding reaches nodal point 15 (at 90 seconds), at a position of approximately 200°C. This temperature monitoring provides valuable insights into the dynamic heat distribution during welding.

In the context of thermal distribution, the temperature gradient near the welding heat source is minimal, resulting in rapid changes in the temperature field. Conversely, as one moves away from the center of the welding heat source, the temperature gradient becomes more pronounced, leading to a more gradual alteration in the temperature field (Ye et al., 2023).

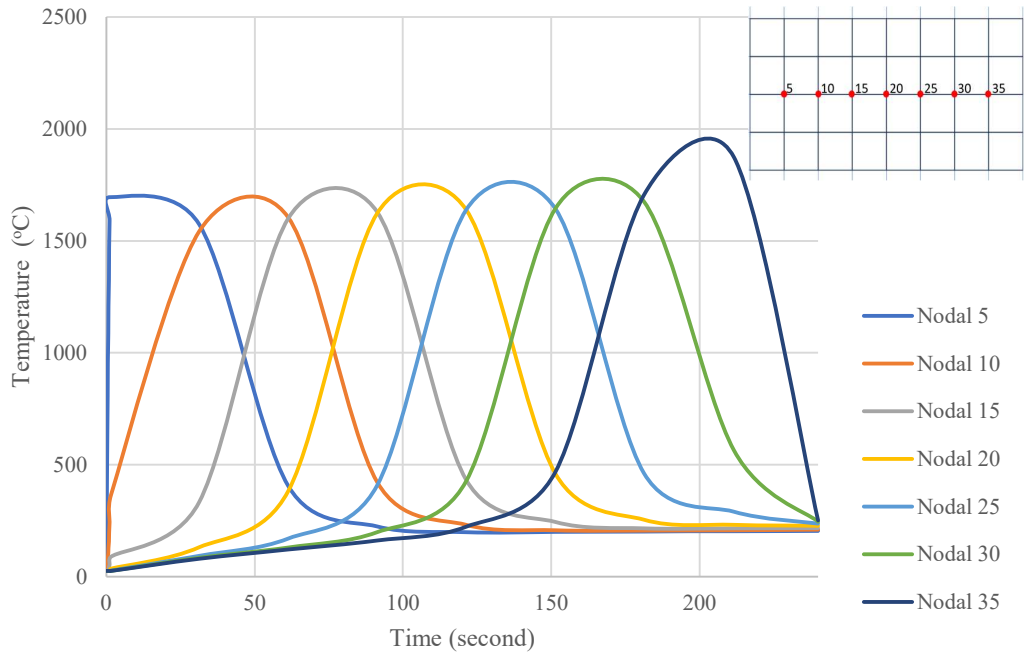

Figure 3. Temperature monitoring at nodes each 5 mm

Stress during welding

Referring to Figure 4, when the temperature reaches its peak during welding, residual stresses emerge, and they approach the melting point of the steel. These residual stresses predominantly manifest both longitudinally and transversely. Notably, the magnitude of transverse residual stress is approximately one-third of the longitudinal residual stress (Ye et al., 2023). This study, however, exclusively focuses on the longitudinal direction, as transverse effects are disregarded. The investigation is primarily concerned with assessing the cross-section's behavior during welding under axial tensile loading conditions.

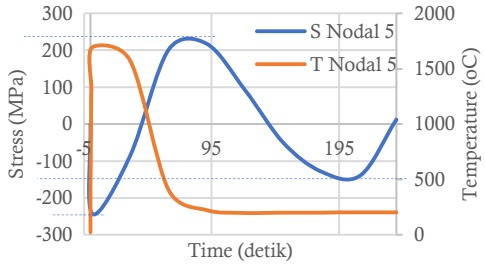

(a)

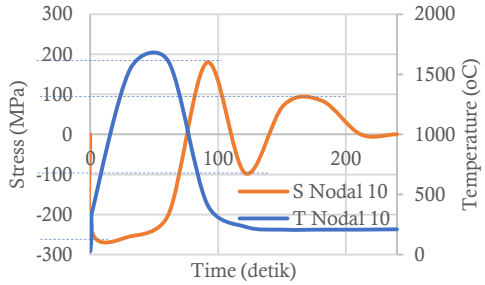

(b)

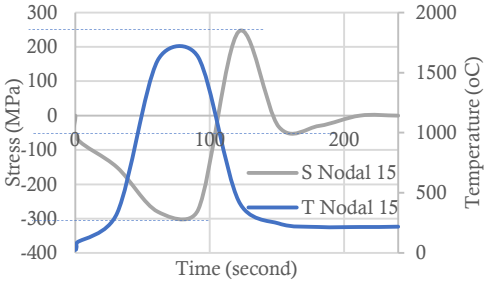

(c)

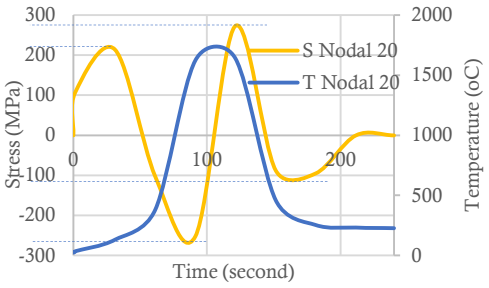

(d)

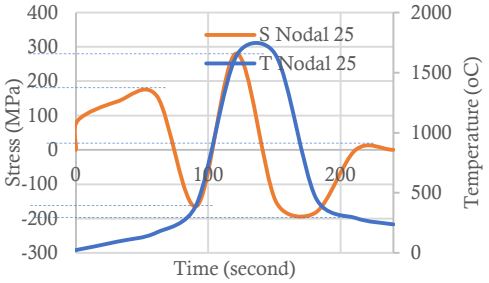

(e)

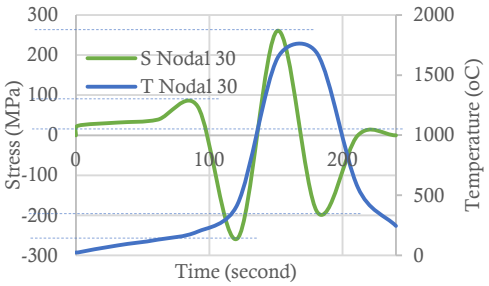

(f)

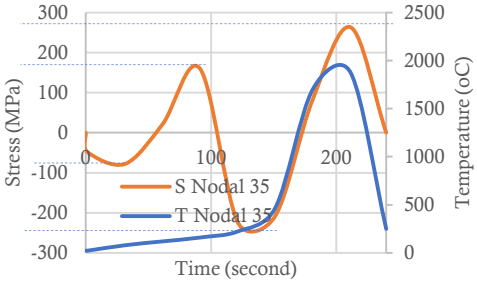

(g)

Figure 4. Stress to time and temperature to time relationship during welding ((a) to (g) as nodes refer to welding path as mentioned in Figure 2)

Ordinary low-carbon steel typically exhibits a yield strength between 240 and 250 MPa. Upon a closer examination of the welding process along the welding path, it becomes evident that the temperature attains its maximum during the welding operation. At the same time, concomitantly, the residual stress within the material nears the yield point. In general, it is essential to note that in certain instances, these residual stresses can induce substantial plastic deformation, resulting in the warping and distortion of the welded object. Effective management of these factors is essential to ensuring welded components structural integrity and dimensional stability.

Width of HAZ

Calculating the width of the heat-affected zone (Tabel 2) holds significant importance as it provides valuable insights into the extent of the affected section compared to the remainder. By determining the width of the HAZ, how much of the material has changed due to the welding process can be precisely gauged, which in turn helps to ascertain how much of the base metal remains unaffected. This knowledge is crucial for gaining insight into the structural integrity and attributes of the welded joint, facilitating the identification of the base metal segment that has preserved its original properties. The following data represents the heat-affected zone width analysis using equation (1).

Tabel 2. Width of heat affected zone to temperature data

Y (mm)	Tp (°C)
0.0	1540.00
2.5	1038.85
5.0	786.84
7.5	635.17
10.0	533.87
12.5	461.41
15.0	407.02
17.5	364.68
20.0	330.79
22.5	303.05
25.0	279.92
27.5	260.35
30.0	243.56
32.5	229.02
35.0	216.28
37.5	205.05
40.0	195.06
42.5	186.12
45.0	178.07

The stress-strain curves depicted in Figure 5 illustrate how S275 steel, as per Eurocode 3, experiences a gradual decline in both its strength and stiffness with increasing temperatures. This alteration becomes noticeable at relatively low temperatures, starting from 300°C, even though the steel's melting point is considerably higher at around 1500°C. The material retains only 23% of its strength at 700°C, which further reduces to 11% at 800°C, and ultimately reaches 6% at 900°C (Lu et al., 2003).

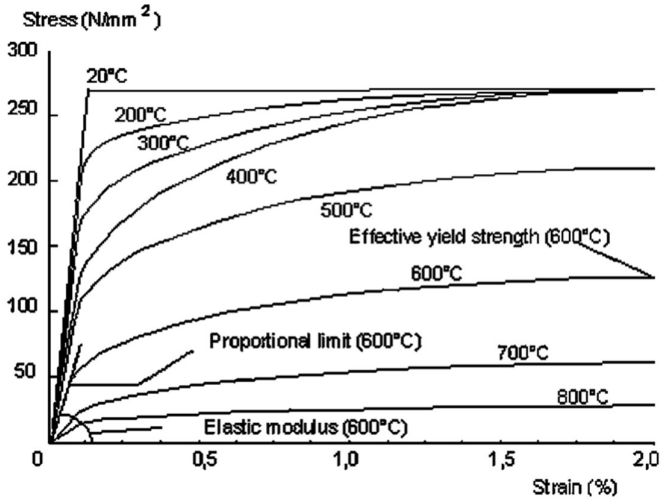

Figure 5. Reduction of stress-strain properties with temperature for S275 steel (Lu et al., 2003)

The mechanical characteristics of steel at a standard temperature of 20°C are assumed by the specifications outlined in Eurocode 3, Part 1.1, SNI 1729-2019 or AISC standard, which is typically used for conventional design purposes. The modified stress-strain relationship at elevated temperatures is observed by (Lu et al., 2003) within a heating range spanning 2 to 50 K/min. Table 3 presents the reductio factors for adequate yield strength, proportional limit, and the slope of the linear elastic range.

Table 3. Reduction factors for stress-strain relationship of steel at elevated temperatures (Lu et al., 2003)

Steel temperature	Reduction factors at temperature relative to the value at 20ºC		
	Effective yield strength	Proportional limit	Slope of the linear elastic range
θ_a	$k_{y,\theta} = f_{y,\theta} / f_y$	$k_{p,\theta} = f_{p,\theta} / f_y$	$k_{E,\theta} = E_{a,\theta} / E_a$
20	1.000	1.0000	1.0000
100	1.000	1.0000	1.0000
200	1.000	0.8070	0.9000
300	1.000	0.6130	0.8000
400	1.000	0.4200	0.7000
500	0.780	0.3600	0.6000
600	0.470	0.1800	0.3100
700	0.230	0.0750	0.1300
800	0.110	0.0500	0.0900
900	0.060	0.0375	0.0675
1000	0.040	0.0250	0.0450
1100	0.020	0.0125	0.0225
1200	0.000	0.0000	0.0000

Note: For intermediate values of the steel temperature, linear interpolation may be used

Steel elements do not change in their mechanical properties when subjected to temperatures below 200°C. Above 200°C, reduced mechanical properties must be used, as specified in Table 2, where the proportional limit and slope of the elastic range decrease. Therefore, based on the information provided in Table 1, it is justifiable to equate the behavior of a four mm-thick steel element to that of its base metal when welding is performed at distances exceeding 40 mm from the heat-affected zone.

This study conducted an analysis and simulation using steel plates of varying thicknesses. The primary objective of these simulations was to determine the width of the affected zone. This affected zone (measured from the welding point), in the context of this study, pertains to the specific region experiencing temperature fluctuations from 1500°C down to 200°C during the welding process. As the simulations progressed, distinct trends were observed for each steel thickness. It was noted that an increase in steel plate thickness (as shown in Figure 6) corresponded to a reduction in the width of the affected zone.

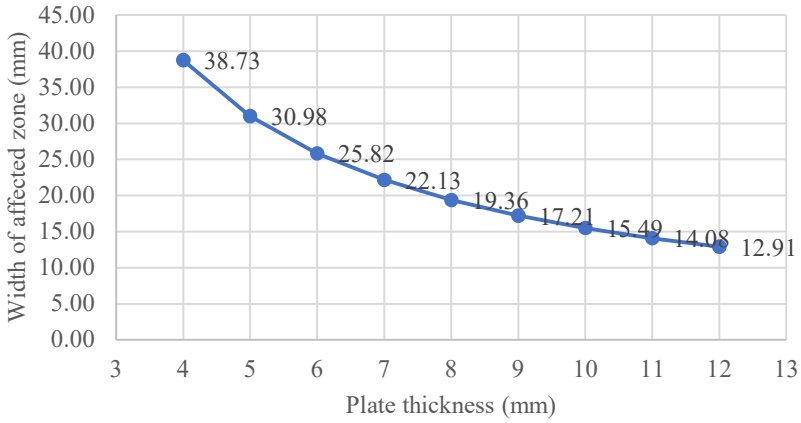

Figure 6. Width of affected zone related to plate thickness during welding

Welding Distortion

All fusion-welding techniques create a weld by translating a molten pool along the joint. The heated metal shrinks upon cooling, inducing residual stresses and distortion in the welded structure. These stresses give rise to both longitudinal and rotational distortion. Longitudinal distortion is typically not a significant concern in many instances. A welded beam with an asymmetric weld, particularly concerning the cross-sectional center of gravity, may exhibit bending as an illustrative example of this type of distortion (Weman, 2003).

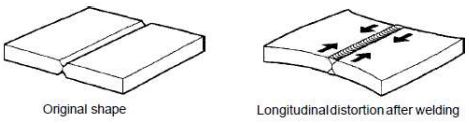

Figure 7. Longitudinal distortion (Weman, 2003)

A cooling process characterizes the post-welding phase after the welding operation. This cooling phase is essential as it transitions from the high-temperature welding environment to ambient conditions. During the welding, expansion forces emerge, primarily driven by the distortion effects stemming from thermal expansion. These forces can lead to changes in the shape and size of the welded components. In contrast, as the welded structure cools down, it experiences shrinkage forces generated by the shrinkage effect. These cooling-induced forces counteract the earlier expansion forces (Ozcatalbas & Vural, 2009).

As observed in Figure 7, the transition from the welding phase to the cooling phase in steel welding brings about notable changes in stress distribution within the welded structure. During the welding phase, the nodes typically encounter stress consistently, often appearing as expansion forces induced by the thermal expansion effects. However, once the welding is complete and the cooling phase commences, the nodes shift towards experiencing opposing stresses. These stresses are attributed mainlt to the cooling-induced shrinkage forces as the material contracts.

Conclusion

When utilizing a four-mm-thick steel plate, the outcome generates an affected zone with a width of approximately 38.73 mm. In contrast, simulations with 5 mm, 6 mm, 7 mm, 8 mm, 9 mm, 10 mm, 11 mm, and 12 mm thicknesses result in progressively narrower affected zones. These simulations yield affected zone widths of approximately 30.98 mm, 25.82 mm, 22.13 mm, 19.36 mm, 17.21 mm, 15.49 mm, 14.08 mm, and 12.91 mm, respectively.

The thickness of a steel plate plays a pivotal role in determining the width of the affected zone, with thicker plates resulting in a narrower affected zone. This relationship allows for estimating the remaining section behavior akin to the base metal. In the context of welding, it is imperative to consider welding distortion as a significant phenomenon when incorporating welding into structural connections.

References

Ahola, A., Lipiäinen, K., Lindroos, J., Koskimäki, M., Laukia, K., & Björk, T. (2023). On the Fatigue Strength of Welded High-Strength Steel Joints in the As-Welded, Post-Weld-Treated and Repaired Conditions in a Typical Ship Structural Detail. *Journal of Marine Science and Engineering*, 11(3). https://doi.org/10.3390/jmse11030644

Andreotti, M., Brondi, C., Micillo, D., Zevenhoven, R., Rieger, J., Jo, A., Hettinger, A. L., Bollen, J., Malfa, E., Trevisan, C., Peters, K., Snaet, D., & Ballarino, A. (2023). SDGs in the EU Steel Sector: A Critical Review of Sustainability Initiatives and Approaches. *Sustainability (Switzerland)*, 15(9). https://doi.org/10.3390/su15097521

Arifin, A., & Hendrianto, M. (2018). Pengaruh Arus dan Jarak Kampuh Pengelasan Terhadap Distorsi Sambungan Pelat Baja Karbon Rendah Dengan Menggunakan SMAW. *Flywheel: Jurnal Teknik Mesin Untirta* Volume IV Nomor 1, April 2018 http://dx.doi.org/10.36055/fwl.v1i1.3288

Fahmy, F., Abdel-Samad, A. G., El-Dakroury, A. A. A., Khalil, A., El-Sawy, M. A. (2019). Fire resistance of welded connections: A review. *Journal of Constructional Steel Research*, 160: 105753.

Jeffus, L. (2017). *Welding Principles and Applications Eighth Edition*. www.cengage.com/highered

Khan, K., Chen, Z., Liu, J., & Javed, K. (2023). State-of-the-Art on Technological Developments and Adaptability of Prefabricated Industrial Steel Buildings. *Applied Sciences (Switzerland)* (Vol. 13, Issue 2). MDPI. https://doi.org/10.3390/app13020685

Kou, S. (2003). *Welding Metallurgy Second Edition*.

Li, G., Li, Y., Yang, Y., Liu, J., Zhang, J., Wang, P, Yang, Z. (2020). Fire performance of steel trusses considering thermal expansion and bowing effects. *Journal of Building Engineering*, 127: 101167.

Liew, J. Y. R., Chua, Y. S., & Dai, Z. (2019). Steel concrete composite systems for modular construction of high-rise buildings. *Structures*, 21, 135–149. https://doi.org/10.1016/j.istruc.2019.02.010

Liu, X., Cheng, Y., Zhang, J., Wang, X. (2019). Influence of residual stresses on fire performance of welded joints in steel structures. *Advances in Steel Structures*, 11(4): 389-405.

Lu, Wei., Mäkeläinen, Pentti., & Painopörssi). (2003). Advanced Steel Structures - Fire and Fatigue Design. Helsinki University of Technology.

Nursani, R., Syarif, M., & Huseiny, A. (2020). Analisis Numerik Sambungan Las Struktur Baja Dengan Menerapkan Variasi Layout Las. *Akselerasi: Jurnal Ilmiah Teknik Sipil* 2(1).

Ozcatalbas, Y., & Vural, H. I. (2009). Determination of optimum welding sequence and distortion forces in steel lattice beams. *Journal of Materials Processing Technology*, *209*(1), 599–604.

https://doi.org/10.1016/j.jmatprotec.2008.02.051

Rezaeian A, Keshavarz M, Hajjari E (2020). Mechanical properties of steel welds at elevated temperatures. *Journal of Constructional Steel Research*, 167: 105853.

Roy, K., Dani, A. A., Ichhpuni, H., Fang, Z., & Lim, J. B. P. (2022). Improving Sustainability of Steel Roofs: Life Cycle Assessment of a Case Study Roof. *Applied Sciences (Switzerland),* 12(12). https://doi.org/10.3390/app12125943

Nia, S. P. S., & Kulatunga, U. (2017). Safety and security of hospitals during natural disasters: Challenges of disaster managers. *International Journal of Safety and Security Engineering*, 7(2), 234–246. https://doi.org/10.2495/SAFE-V7-N2-234-246

Szymczak, T., Makowska, K., & Kowalewski, Z. L. (2020). Influence of the welding process on the mechanical characteristics and fracture of the s700mc high strength steel under various types of loading. *Materials*, 13(22), 1–17. https://doi.org/10.3390/ma13225249

Wang, Y., Li, Y. Q., Wang, H. Y., Y. C., Liu, Wu, X. L. (2019). Experimental and numerical study on fire performance of beam-to-column connections with high-strength bolts. *Engineering Structures*, 181: 137-153.

Weiss, S., Pense, A. W., Reynolds, Jr., S. D., Weisman, C., Betz, I. G., Frohlich, R. L., Saperstein, Z. P., Somers, R. E., Stern, I. L., Telford, R. T., & Wilcox, W. L. (1976). *Fundamentals of Welding*.

Weman, K. (2003). *Welding processes handbook*. Woodhead Pub.

Wibowo, A., Purnowidodo, A., & Andika, H. P. (2012). Distribusi dan Interaksi Tegangan Sisa antar Lubang Setelah Proses Cold Expansion Hole. *Jurnal Rekayasa Mesin*, 3(3), 372–379.

Wu, Y., Li, Z., Zhang, Y., Zhang, J., Wang, J. (2021). Experimental and numerical investigation of thermal expansion and out-of-plane deformations of steel beams under fire. *Fire Safety Journal*, 146: 105216.

Ye, Z., Liu, J., Xie, C., & Zhang, S. (2023). Numerical Simulation of Welding Temperature Field, Stress Field, and Strain Field of Fillet Joint in Different Welding Sequence. *Journal of Physics: Conference Series*, 2541(1), 012003. https://doi.org/10.1088/1742-6596/2541/1/012003

Yu, J., Wang, X.L., Zhang, J.Y., Liu, Y.C., Zhang, S.Y., Yang, L. (2018). Buckling behavior of steel columns under fire conditions: A parametric study. *Engineering Structures*, 165: 56-71.